

## Supplementary Information for:

### Optogenetic stimulation of the auditory pathway

Victor H. Hernandez<sup>1,2,§</sup>, Anna Gehrt<sup>1,\*</sup>, Kirsten Reuter<sup>1,2,\*</sup>, Zhizi Jing<sup>1,3,\*</sup>, Marcus Jeschke<sup>1</sup>,  
Alejandro Mendoza Schulz<sup>1</sup>, Gerhard Hoch<sup>1,2</sup>, Matthias Bartels<sup>4</sup>, Gerhard Vogt<sup>2,5</sup>, Carolyn W.  
Garnham<sup>2,5</sup>, Hiromu Yawo<sup>6</sup>, Yugo Fukazawa<sup>7</sup>, George J. Augustine<sup>8,9</sup>, Ernst Bamberg<sup>10</sup>,  
Sebastian Kügler<sup>11</sup>, Tim Salditt<sup>4</sup>, Livia de Hoz<sup>12</sup>, Nicola Strenzke<sup>3</sup>, Tobias Moser<sup>1,2,#</sup>

Contains:

- Supplementary Table 1: vectors tested for virus-mediated gene transfer using transuterine injections into the embryonic otocyst
- Supplementary Figure 1: oABR evoked by intracochlear stimulation with single channel  $\mu$ -LED-implants
- Supplementary Figure 2: ABR evoked by different stimulation modalities
- Supplementary Figure 3: Local field potential recordings in the inferior colliculus
- Supplementary Figure 4: Tonotopic gradient in the IC – an acoustic calibration
- Supplementary Figure 5: aABR hearing thresholds in C57Bl/6 mice
- Supplementary Figure 6: Optical activation of the auditory pathway in ChR2-transgenic rats
- Supplementary Figure 7: Acoustic response properties of light- and sound-sensitive putative SGN
- Supplementary Figure 8: x-ray tomography: Estimation of available space for an intracochlear implant
- Supplementary Figure 9: Simulation of intracochlear  $\mu$ -LED-based optical stimulation
- Supplementary Figure 10: Stimulus-rate dependence of oABR amplitude
- Supplementary Movie 1: x-ray tomography: tonotopic position of cochlear stimulation

**Table S1**

Virus	Sero- type	Promoter	ChR2 variant	Reporter	Source	Expression in SGN	Number of animals tested at postnatal age groups			
							P7*	P14*	P21*	>1month
AAV	6	HSYN	ChR2 (L132C)	YFP	<sup>2)</sup>	yes, good	9	6		21 <sup>††</sup>
AAV	6	HSYN	ChR2 (H134R)	YFP	<sup>3)</sup>	yes, very weak	8	3	3	2
AAV	1/2	CAG	ChR2	YFP	<sup>4)</sup>	yes, very weak	5	5		
AAV	2/1	CMV	ChR2 (H134R)	RFP	<sup>1)</sup>	no	3			3
AAV	2/7	LTR	ChR2	YFP	<sup>1)</sup>	no	**			5
AAV	2/1	CAG	ChIEF	tdTomato	<sup>4)</sup>	no	4	4	3	
AAV	5	CaMKIIa	ChR2 (E123A)	YFP	<sup>5)</sup>	no	10	12	4	8
HSV		Ef1a	ChR2 (E123T/H134R)	YFP	<sup>5)</sup>	no	<sup>†</sup> 4	3	3	
HVJ-E		HSYN	ChR2	YFP	<sup>6)</sup>	no	6	4	9	
HVJ-E		HBA	-	GFP	<sup>6)</sup>	no	7	4	7	

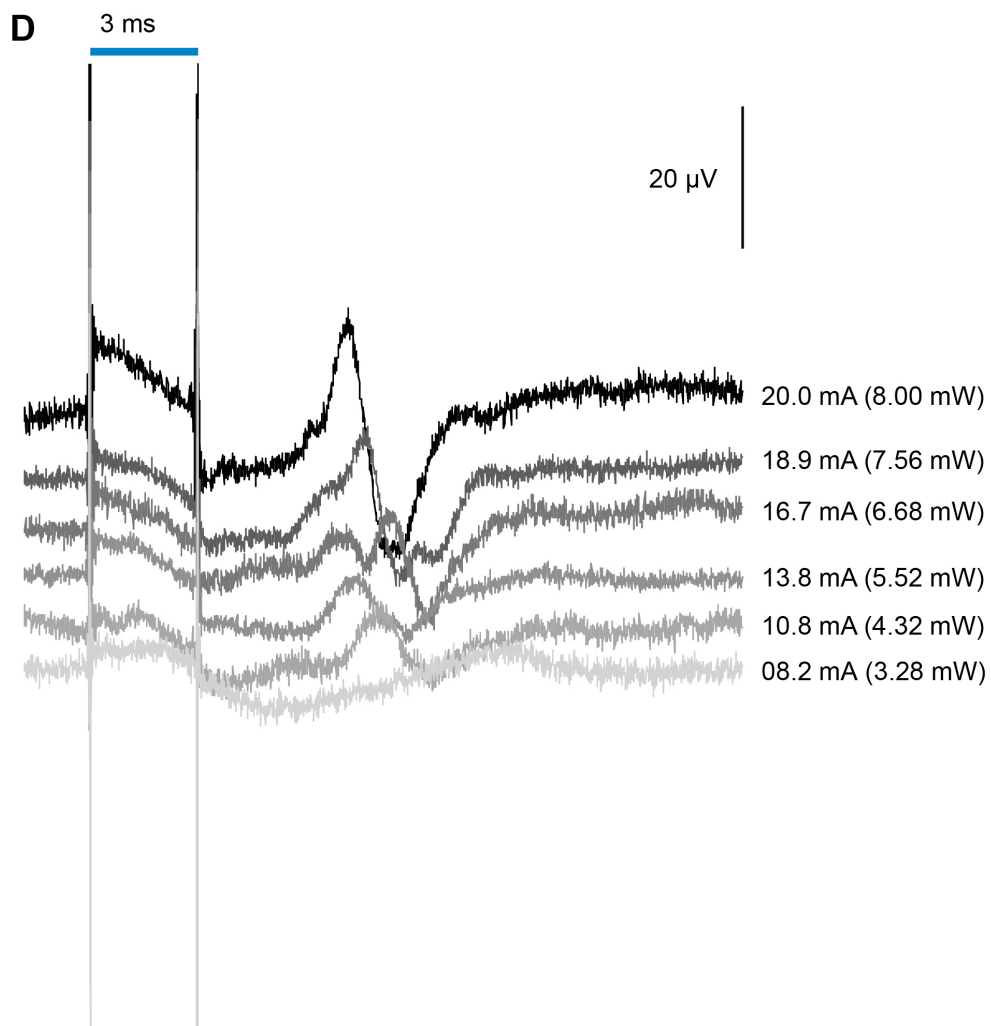
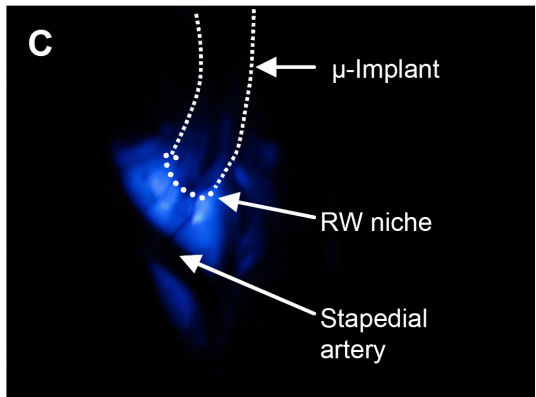
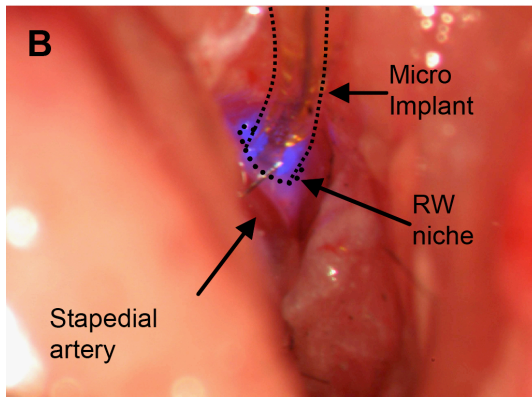
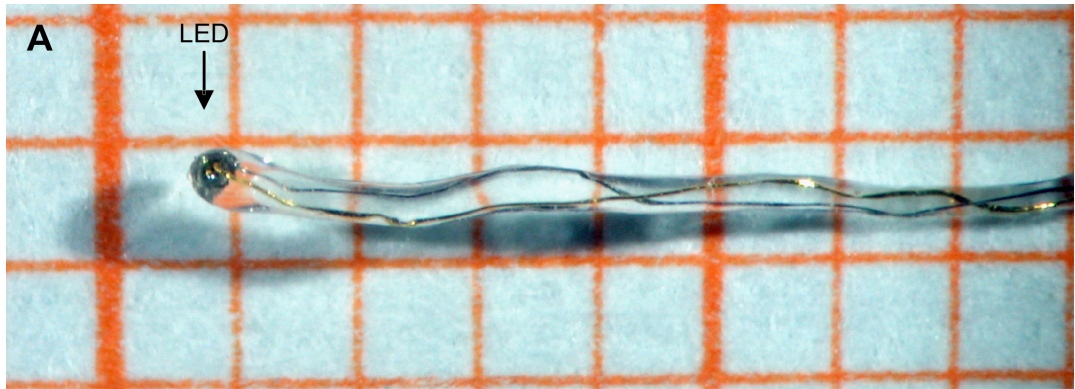
\* ± 1 day

\*\* no fluorescence was found in acute preparations of P5 – P9 animals, immunohistochemistry not examined in younger animals

<sup>†</sup> Additional 4 animals were tested P1 and P2 and 2 more at P5

<sup>††</sup> Animals that have undergone surgery for oABR recordings

<sup>1)</sup> Department of Biophysical Chemistry, Max Planck Institute of Biophysics Frankfurt, virus production by Penn vector core; <sup>2)</sup> Viral Vectors Laboratory, Dept. of Neurology, Göttingen University Medical School; <sup>3)</sup> Institute of Physiology I-Neurophysiology, Westfälische Wilhelms-University Münster; <sup>4)</sup> Molecular Neurobiology, European Neuroscience Institute Göttingen; <sup>5)</sup> Department of Bioengineering, Department of Psychiatry and Behavioral Sciences, Stanford University; <sup>6)</sup> HVJ envelope vector commercially available: GenomeONE®

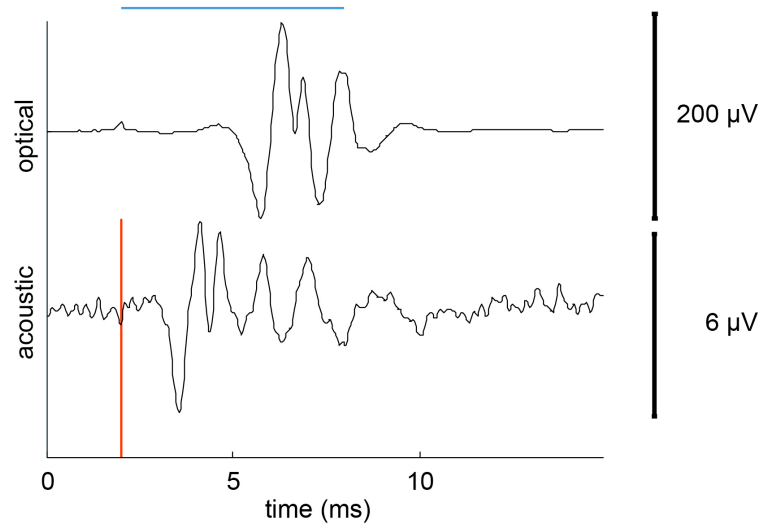
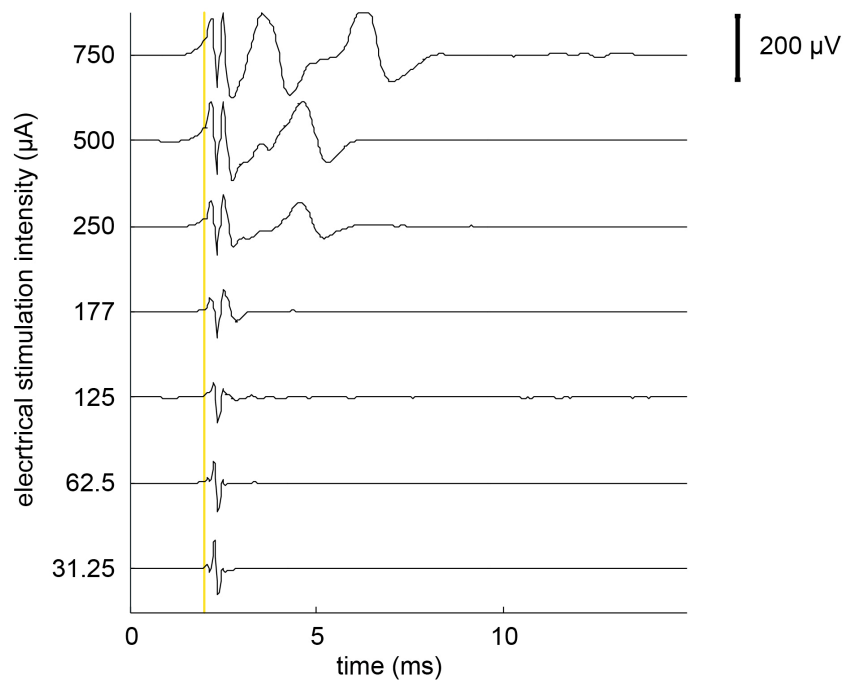
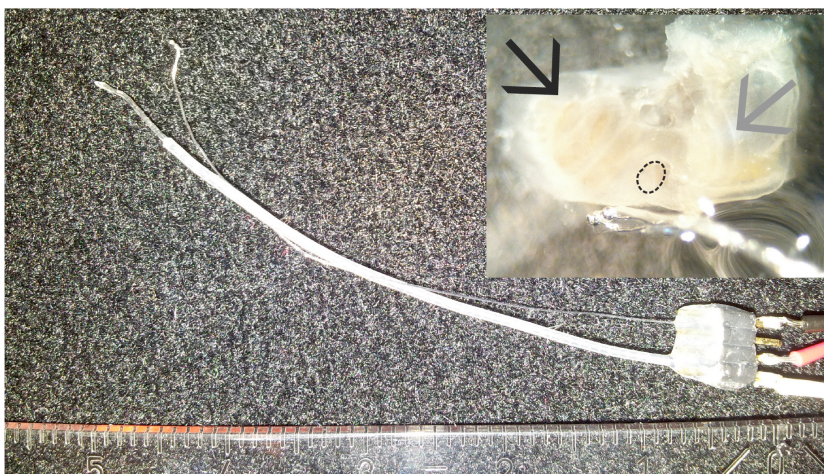


**Figure S1 oABR evoked by intracochlear  $\mu$ -LED-implant**

**A**, Photograph of an optogenetic microimplant with a  $\mu$ -LED embedded in silicone on 1 mm engineering graph paper.

**B** (in light) and **C** (in dark), Intracochlear microimplant in situ, inserted through the round window (RW), shining blue light through the bone surrounding the round window.

**D**, oABR evoked by an intracochlear  $\mu$ -LED implant at varying stimulation current amplitudes. oABR traces for different stimulus intensities were offset vertically for better visibility.

**A****B****C**

**Figure S2 ABR evoked by different stimulation modalities**

**A**, oABR evoked by 6 ms of 24 mW 473 nm laser light applied at 6 Hz via an intracochlear 250  $\mu$ m optical fiber inserted through the round window (as used in Figure 5), aABR in response to 80 dB click stimulation (as used in Figure 1). Colored bars indicate stimuli.

**B**, eABR evoked by biphasic current pulses of various amplitudes (80  $\mu$ s pulse width, 20  $\mu$ s pulse interval) applied with an intracochlear electrode (monopolar stimulation, see image in (C)) with the reference placed in the neck musculature (as used in Figure 5).

**C**, Rodent cochlea implant for electrical stimulation used in the study. A silver wire electrode embedded in silicone was inserted into the cochlea via the round window to evoke local field potentials in the ICC. Scale in cm. The inset shows a 25x magnification of the cochlear ending of the implant next to an explanted mouse cochlea in 2,2'-Thiodiethanol (Sigma-Aldrich, St. Louis, MO, USA). The black arrow points to the cochlear apex, the grey arrow points to a semicircular canal. The round window is indicated by the dashed-lined circle.

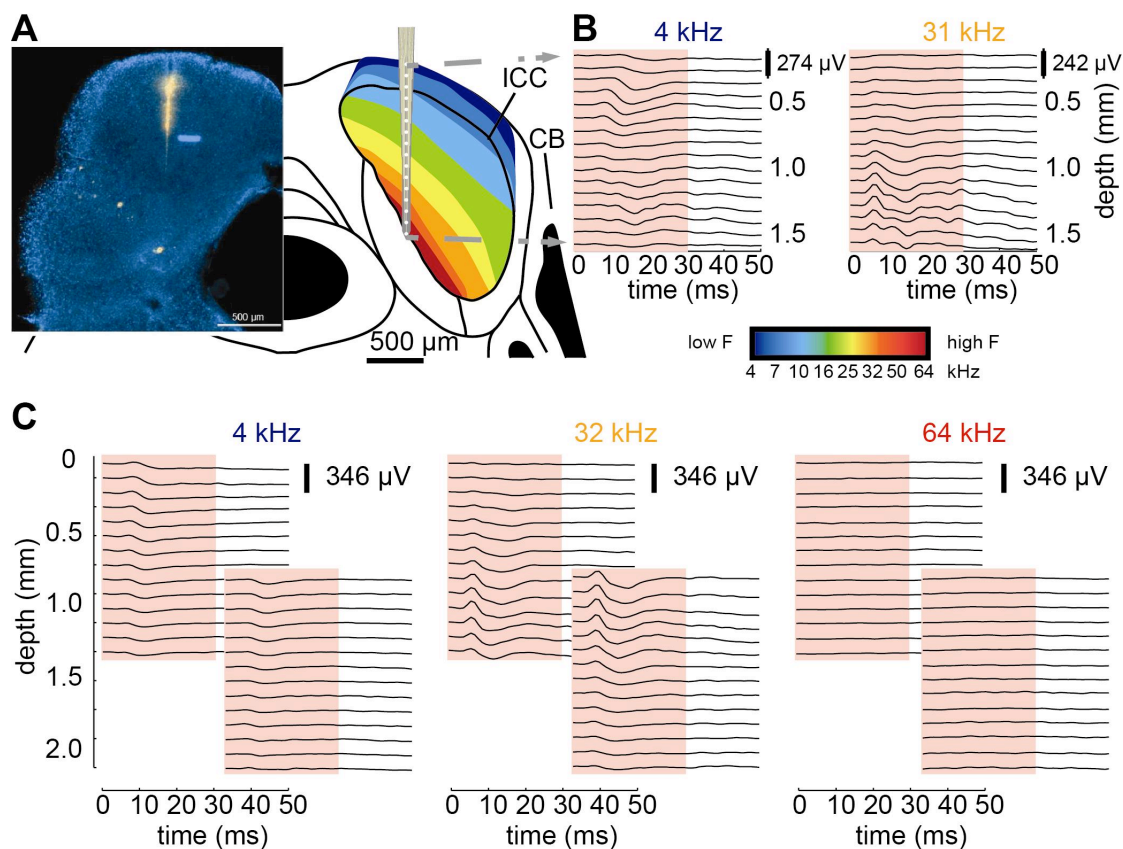


**Figure S3 Local field potential recordings in the inferior colliculus**

**A,** Histological image of an electrode track targeting the left central nucleus of the inferior colliculus (ICC). A frontal midbrain slice after recording with an electrode coated with the fluorescent dye DiI (1) is shown on the left. The structure of neuronal tissue was visualized by staining the section with DAPI. To the right a schematic representation of the recording situation with the approximate electrode position is shown. The tonotopy of mouse ICC is color-coded (modified from (2)). CB: cerebellum

**B,** Representative LFPs to a 4 kHz and a 31 kHz tone burst (80dB (SPL), shaded area indicates stimulus timing) with the top-most channel of the recording electrode located at the surface of the IC. While the presentation of a 4 kHz tone led to the strongest LFP at a depth of  $\sim 0.5$  mm, the presentation of a 31 kHz tone evoked the strongest response at  $\sim 1.2$  mm revealing the dorsal-to-ventral tonotopic gradient (low to high frequencies) of the ICC.

**C,** Evoked LFPs after stimulation with 4, 32 and 64 kHz recorded at two overlapping depth locations. With the top-most channel located at the surface of the ICC (upper panels) a clear

tonotopic gradient was observed with 4 kHz leading to more superficial activation than 32 kHz. No discernible response was detected after stimulation with 64 kHz. To exclude the possibility that higher frequencies led to an activation of the ICC in deeper layers the recordings were repeated at a depth of 0.8 mm (top-most channel). After the electrode was advanced the pattern of activation seemed merely shifted for 0.8 mm without changing the response shape. Again no response was observed after stimulation with 64 kHz. This result was expected due to the well documented high frequency hearing loss of the C57Bl/6 mouse strain used in this study ((3), see Figure S5).

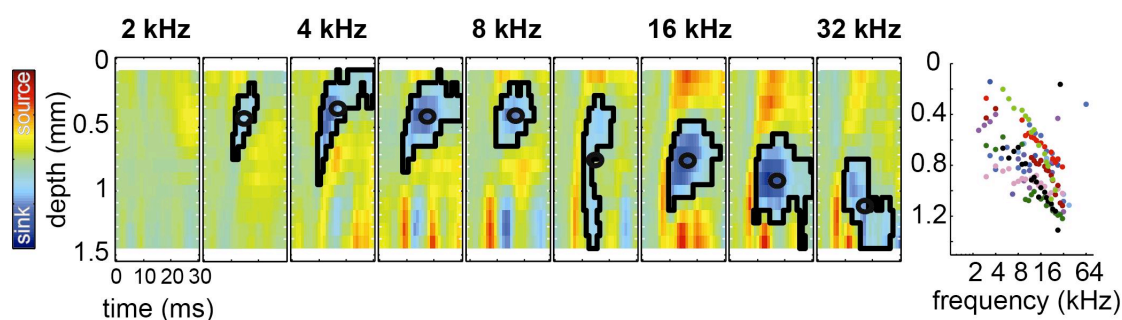


**Figure S4 Tonotopic gradient in the IC – an acoustic calibration**

Frequency gradients along linear, multielectrode arrays were used to calibrate the location of responses to electrical and optical stimulation within the tonotopic map of the ICC (4). Representative CSDs evoked by tone bursts of varying frequencies (quarter octave steps were presented; individual CSD panels show half octave steps for better visibility) of one animal are shown. Sinks were plotted in blue, sources in red. The strongest of the significant sinks were outlined in black with their centroid indicated by black open circles. A positive correlation between increasing depth of the sink centroids and tone burst frequency was observed. Responses following stimulation with frequencies below 3 and above 32 kHz were rare.

**Right panel,** Recording depth of centroid (quarter octave steps were analyzed) is illustrated as a function of stimulation frequency for different animals (denoted by diverse colors). Within one and across all experiments ( $n = 9$ ) responses to high frequency stimuli were observed in deep layers of the ICC whereas low frequency stimuli led to an activation of more superficial layers. The centroid depth increased with increasing stimulation frequency (4 kHz centroid:  $\sim 0.4$  mm depth; 32 kHz centroid:  $\sim 1.2$  mm depth). The progression as well as the absolute depth of the centroid locations was quantitatively similar to published single unit data (5–7).

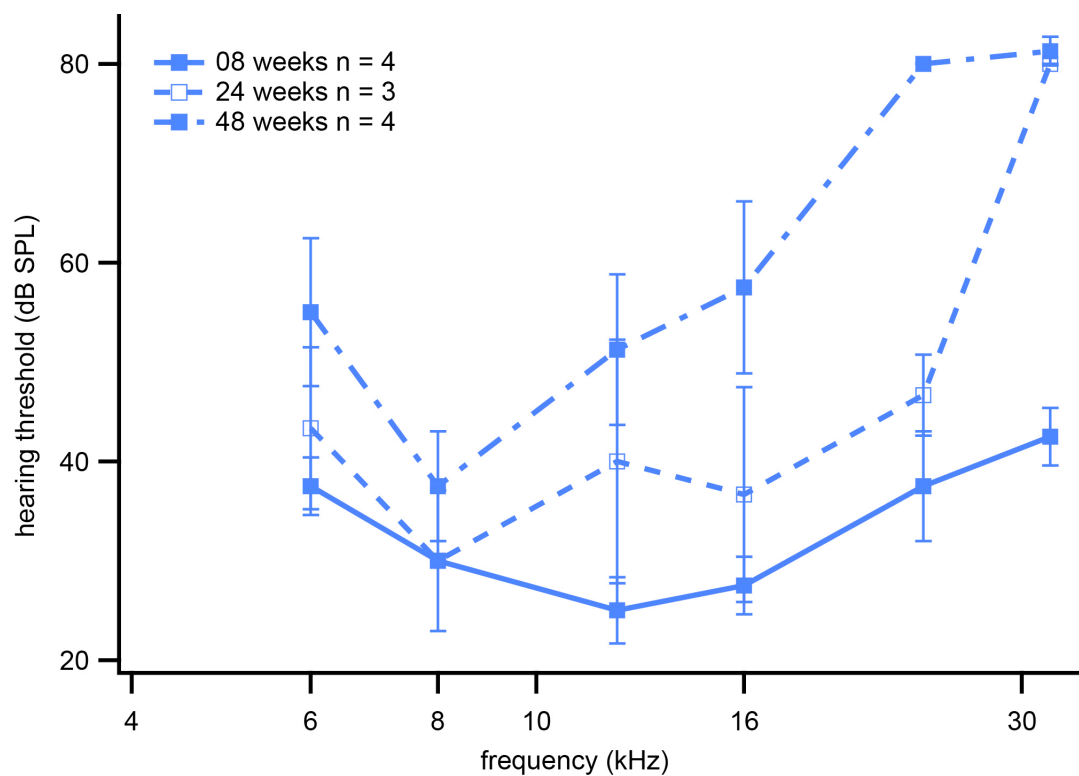


**Figure S5 aABR hearing thresholds in C57Bl/6 mice**

Averaged threshold of C57Bl/6 mice in three groups of different age are shown. While the threshold amounts to 40 dB (SPL) for 32 kHz in 8-week-old mice thresholds increase with age to 80 dB (SPL) in 48 week old animals. As a high frequency hearing loss is expected from 16 weeks of age, optical and electrical stimulation were compared to a 31 kHz tone burst.

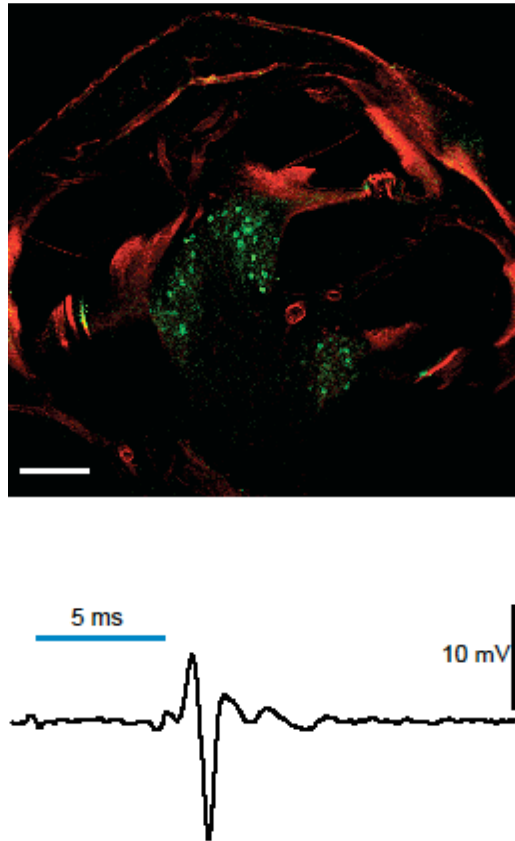


**Figure S6 Optical activation of the auditory pathway in ChR2-transgenic rats**

**Upper panel,** expression of ChR2 in SGNs as shown by immunolabelling for GFP and phalloidin-AF-568 labeling of actin in a longitudinal section of an entire rat cochlea. ChR2 is expressed only in the spiral ganglion neurons, scale bar: 200  $\mu\text{m}$ .

**Lower panel,** representative oABR in response to rectangular 5 ms long blue laser stimulation ( $4.4 \text{ mW/mm}^2$  and 5 Hz, average of 50 trials).

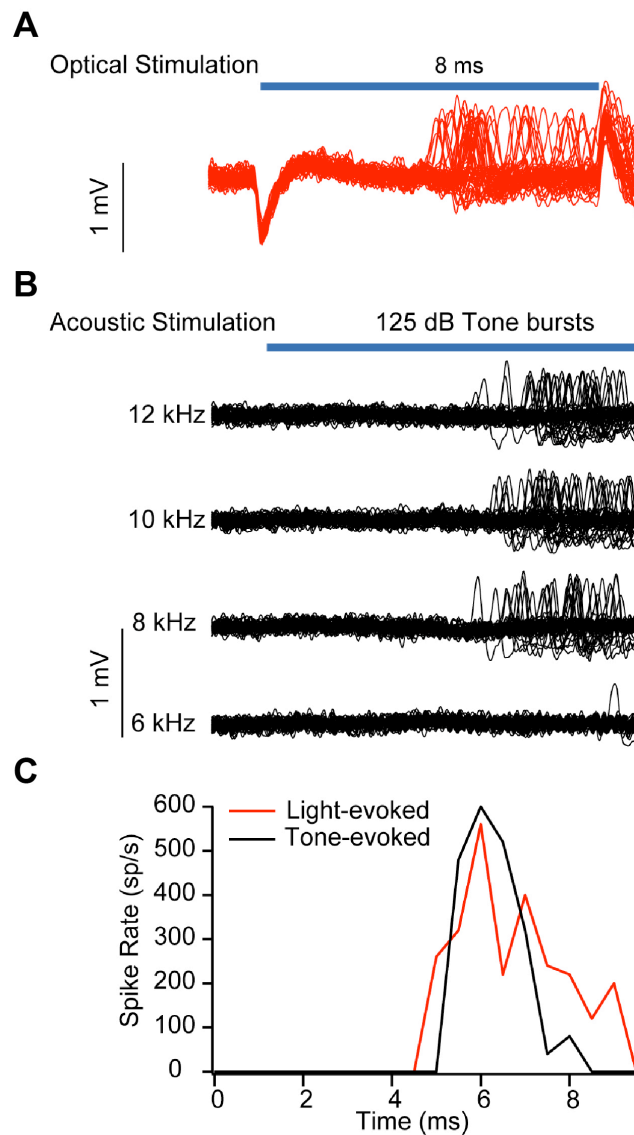


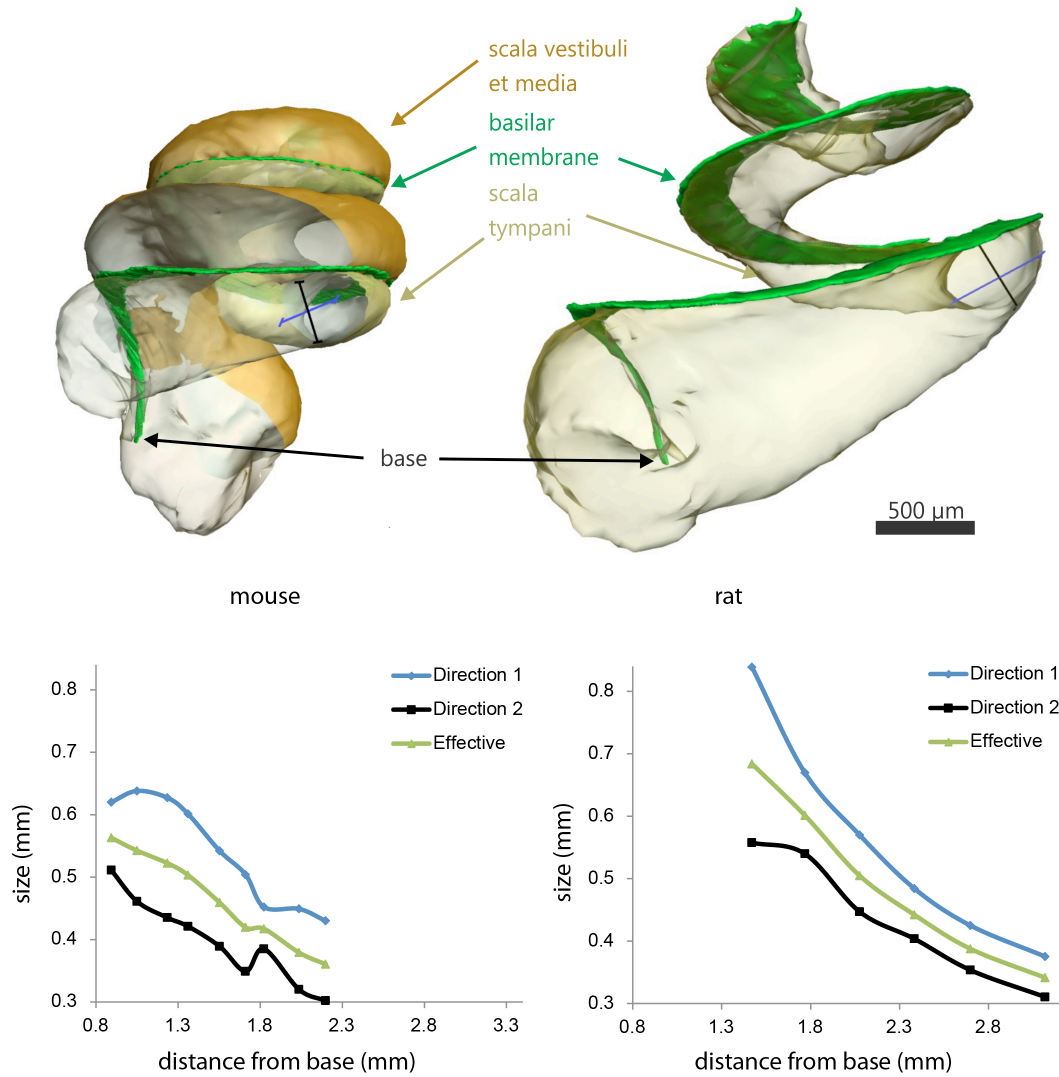
**Figure S7 Acoustic response properties of light- and sound-sensitive putative SGN**

The acoustic and optogenetic stimulation confirmed the activation of neurons in the auditory pathway.

**A**, representative traces showing the responses of a putative SGN to optical stimulation (red traces).

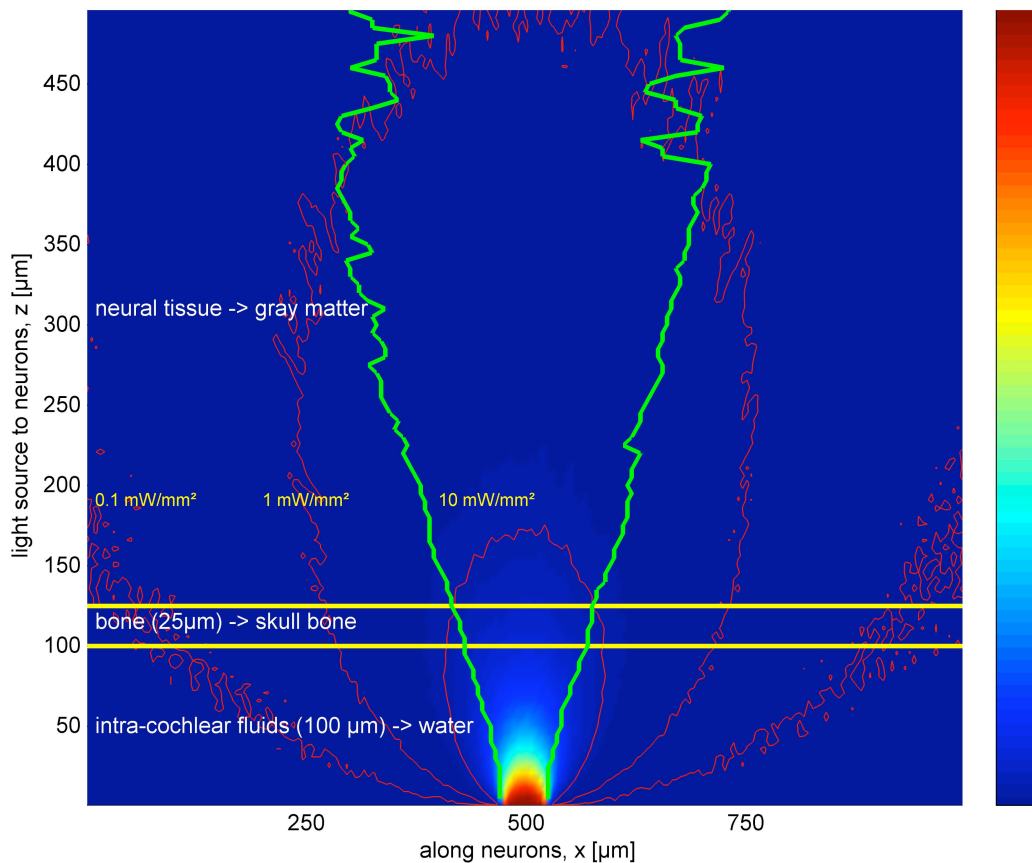
**B**, corresponding acoustic evoked response to tone bursts of different frequencies (black traces).

**C**, corresponding PSTH of light-evoked (8 ms, 22.1 mW, 10 Hz repetition rate) and tone-evoked (8 kHz, 125 dB, 10 Hz repetition rate) responses.



**Figure S8 x-ray tomography: Estimation of available space for an intracochlear implant**

3D-representation of basilar membrane (green), scala vestibuli et media (brown) and scala tympani (fawn) obtained by x-ray phase contrast tomography (only the basilar membrane and scala tympani were traced in the rat cochlea tomography). The size of scala tympani along the basilar membrane was measured as exemplary shown for one position. Blue lines represent the direction with largest width; black is the corresponding orthogonal direction. Both directions along with its geometric mean (green, effective diameter) are shown as a function of the distance from the base.



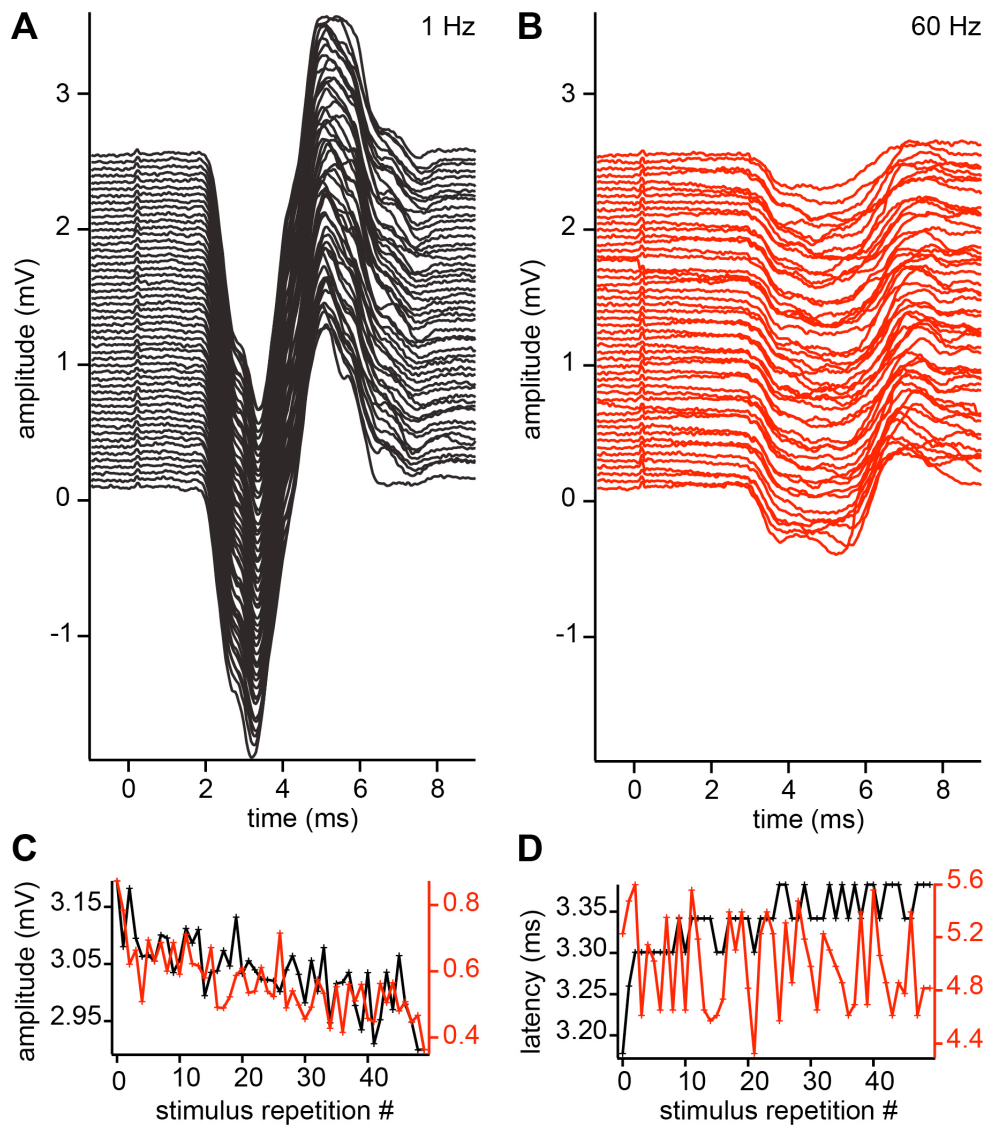
**Figure S9 Simulation of intracochlear  $\mu$ -LED-based optical stimulation**

Fig. S9 displays the result of a simulation of illumination of SGN somata within Rosenthal’s canal by a  $50 \times 50 \mu\text{m}^2$  sized rectangular  $\mu$ -LED (Lambertian emitter) placed in scala tympani in  $100 \mu\text{m}$  proximity facing the medial wall of the mouse cochlea and assuming a total emitted power of 1 mW. A three-layered model was used:  $100 \mu\text{m}$  cochlear fluid,  $25 \mu\text{m}$  bone (medial cochlear wall as measured by x-ray tomography) and  $375 \mu\text{m}$  “nerve tissue” (exceeding the  $175 \mu\text{m}$  mean radial diameter of spiral ganglion in Rosenthal’s canal as measured by x-ray tomography). The irradiance is plotted as colors (look-up table and contour lines for a cross section nominal on the light source surface) and the full width at half maximum of the emitted light beam is depicted as green lines. The red contour lines represent iso-irradiance lines of  $10 \text{ mW/mm}^2$ ,  $1 \text{ mW/mm}^2$  (the irradiance for which we typically found an oABR with wild-type ChR2 when stimulating for 2 ms or longer) and  $0.1 \text{ mW/mm}^2$ . Depending on the stimulation threshold the red contour lines mark the area where stimulation of neurons takes place if the simulation appropriately predicts light propagation in the real tissue situation. Halfway through the spiral ganglion (at approximately  $215 \mu\text{m}$  from the

LED) the full width at half maximum of the beam amounted to approximately  $250 \mu\text{m}$ . When i) assuming this to reflect the average spread of excitation throughout the ganglion and ii) considering that the radius from the central modiolar axis to the middle of the spiral ganglion is approximately half of that from the central modiolar axis to the organ of Corti (to which the peripheral neurites of the stimulated SGNs spread resulting in an arc of  $500 \mu\text{m}$ ) we can use the tonotopic map of the mouse cochlea(8) to predict that the frequency resolution roughly amounts to a third of an octave for this mode of  $\mu\text{LED}$  stimulation. We note that this mode of optical stimulation is less favorable for achieving high frequency resolution than directing the light beam towards the peripheral SGN neurites where they approach the organ of Corti. We chose this mode for a lower estimate of frequency resolution and, because the neurites may degenerate in inner ear disease. Obviously, when reducing the light intensity the radial and lateral spread of excitation will be reduced. Then fewer neurons will be recruited but the frequency resolution will be greater. Therefore, changing light intensity may mimic physiological loudness scaling, where frequency resolution and recruitment of SGN are traded, too.

Simulations used the program package Zemax (Version 12 EE, RadiantZemax, Redmont, WA) employing Henyey-Greenstein bulk scattering. The software was checked by reproducing reported data from other program packages. The data in table 1 of reference(9) was simulated with less than 1 % accuracy. Other data for a more complex situation within the program manual for the software package MCML (table 6.7 in: <http://omlc.ogi.edu/software/mc/mcml/MCman.pdf>) was reproduced with only a 7 % difference for the diffuse transmittance and a 3 % error for the diffuse reflectance.

We performed the simulations using the dimensional information from our x-ray tomography of the mouse cochlea and reported scattering and absorption parameters(10). For the three layered model we used:  $100 \mu\text{m}$  cochlear fluid (no scattering and no absorption),  $25 \mu\text{m}$  bone (medial cochlear wall as measured by x-ray tomography; reported values for skull bone were used: absorption coefficient  $\mu_a = 0.14 \text{ cm}^{-1}$ , scattering coefficient  $\mu_s = 20 \text{ cm}^{-1}$ , anisotropy  $g = 0.87$  from: ref. (10)) and  $375 \mu\text{m}$  “nerve tissue” (approximated by the values for brain gray matter from(11), which are  $\mu_a = 0.07 \text{ mm}^{-1}$  and  $\mu_s = 10 \text{ mm}^{-1}$ , and  $g = 0.88$ ). In all cases the same refractive index value of 1.3 was used. Irradiance was calculated for areas with a  $5 \times 5 \mu\text{m}^2$  pixel size using 1.500.000 rays. 100 areas were investigated parallel to the light source, each having a distance of  $5 \mu\text{m}$  from each other, thus in total covering a three dimensional space with an overall  $5 \times 5 \times 5 \mu\text{m}^3$  grid.



**Figure S10 Stimulus-rate dependence of oABR amplitude**

**A-B**, 50 subsequent oABRs during transcochlear stimulation with a power-LED/lens array at 1 Hz (**A**) or 60 Hz (**B**). Note the smaller amplitude and longer latency for 60 Hz. Traces have been offset for visibility from bottom to top.

**C-D**, Amplitude and latency of the responses in **A** (**black**) and **B** (**red**): only subtle decrease in amplitude and increase in latency during the recording period in ‘quasi’ steady-state.

### **Movie S1 Visualization of the cochlea by high resolution x-ray tomography**

3D-visualisation of an explanted mouse cochlea obtained by x-ray phase contrast tomography showing basilar membrane (green), Rosenthal's canal (blue), cochleostomy (grey), and point markers used to fit a spline curve to identify the position of the cochleostomy relative to the tonotopic map of the cochlea.

### **References**

1. DiCarlo JJ, Lane JW, Hsiao SS, Johnson KO. Marking microelectrode penetrations with fluorescent dyes. *J Neurosci Methods*. 1996;64(1):75–81.
2. Stiebler I, Ehret G. Inferior colliculus of the house mouse. I. A quantitative study of tonotopic organization, frequency representation, and tone-threshold distribution. *J Comp Neurol*. 1985;238(1):65–76.
3. Willott JF. Effects of aging, hearing loss, and anatomical location on thresholds of inferior colliculus neurons in C57BL/6 and CBA mice. *J Neurophysiol*. 1986;56(2):391–408.
4. Snyder RL, Bierer JA, Middlebrooks JC. Topographic spread of inferior colliculus activation in response to acoustic and intracochlear electric stimulation. *J Assoc Res Otolaryngol*. 2004;5(3):305–322.
5. Sanes DH, Constantine-Paton M. The sharpening of frequency tuning curves requires patterned activity during development in the mouse, *Mus musculus*. *J Neurosci*. 1985;5(5):1152–1166.
6. Yan J, Ehret G. Corticofugal reorganization of the midbrain tonotopic map in mice. *Neuroreport*. 2001;12(15):3313–3316.
7. Portfors CV, Mayko ZM, Jonson K, Cha GF, Roberts PD. Spatial organization of receptive fields in the auditory midbrain of awake mouse. *Neuroscience*. 2011;193:429–439.

8. Müller M, von Hünenbein K, Hoidis S, Smolders JWT. A physiological place-frequency map of the cochlea in the CBA/J mouse. *Hear Res.* 2005;202(1-2):63–73.
9. Wang L, Jacques SL, Zheng L. MCML--Monte Carlo modeling of light transport in multi-layered tissues. *Comput Methods Programs Biomed.* 1995;47(2):131–146.
10. Niemz MH. *Laser-Tissue Interactions: Fundamentals and Applications*. Springer; 2007:
11. Bernstein JG et al. Prosthetic systems for therapeutic optical activation and silencing of genetically-targeted neurons. *Proc Soc Photo Opt Instrum Eng.* 2008;6854:68540H.